

On the analogy between photoluminescence and carrier-type reversal in Bi- and Pb-doped glasses

Mark A. Hughes,^{1,*} Russell M. Gwilliam,¹ Kevin Homewood,¹ Behrad Gholipour,²
Daniel W. Hewak,² Tae-Hoon Lee,³ Stephen R. Elliott,³ Takenobu Suzuki,⁴
Yasutake Ohishi,⁴ Tomas Kohoutek,⁵ and Richard J. Curry¹

¹Advanced Technology Institute, Department of Electronic Engineering, University of Surrey, Guildford, GU2 7XH, UK

²Optoelectronics Research Centre, University of Southampton, Southampton SO17 1BJ, UK

³Department of Chemistry, University of Cambridge, Lensfield Road, Cambridge, CB2 1EW, UK

⁴Toyota Technological Institute, 2-12-1, Hisakata, Tempaku, Nagoya 468-8511, Japan

⁵Centre for Materials and Nanotechnologies, Faculty of Chemical Technology, University of Pardubice, CS. Legion's sq. 565, Pardubice 532 10, Czech Republic

*m.a.hughes@surrey.ac.uk

Abstract: Reaction order in Bi-doped oxide glasses depends on the optical basicity of the glass host. Red and NIR photoluminescence (PL) bands result from Bi²⁺ and Bi_n clusters, respectively. Very similar centers are present in Bi- and Pb-doped oxide and chalcogenide glasses. Bi-implanted and Bi melt-doped chalcogenide glasses display new PL bands, indicating that new Bi centers are formed. Bi-related PL bands have been observed in glasses with very similar compositions to those in which carrier-type reversal has been observed, indicating that these phenomena are related to the same Bi centers, which we suggest are interstitial Bi²⁺ and Bi clusters.

©2013 Optical Society of America

OCIS codes: (160.2540) Fluorescent and luminescent materials; (160.6000) Semiconductor materials.

References and links

1. G. W. Chi, D. C. Zhou, Z. G. Song, and J. B. Qiu, "Effect of optical basicity on broadband infrared fluorescence in bismuth-doped alkali metal germanate glasses," *Opt. Mater.* **31**(6), 945–948 (2009).
2. A. N. Romanov, Z. T. Fattakhova, A. A. Veber, O. V. Usovich, E. V. Haula, V. N. Korchak, V. B. Tsvetkov, L. A. Trusov, P. E. Kazin, and V. B. Sulimov, "On the origin of near-IR luminescence in Bi-doped materials (II). Subvalent monocation Bi⁺ and cluster Bi₅³⁺ luminescence in AlCl₃/ZnCl₂/BiCl₃ chloride glass," *Opt. Express* **20**(7), 7212–7220 (2012).
3. M. Peng, D. Chen, J. Qiu, X. Jiang, and C. Zhu, "Bismuth-doped zinc aluminosilicate glasses and glass-ceramics with ultra-broadband infrared luminescence," *Opt. Mater.* **29**(5), 556–561 (2007).
4. Y. Arai, T. Suzuki, Y. Ohishi, S. Morimoto, and S. Khonthon, "Ultrabroadband near-infrared emission from a colorless bismuth-doped glass," *Appl. Phys. Lett.* **90**(26), 261110 (2007).
5. M. Peng, B. Wu, N. Da, C. Wang, D. Chen, C. Zhu, and J. Qiu, "Bismuth-activated luminescent materials for broadband optical amplifier in WDM system," *J. Non-Cryst. Solids* **354**(12-13), 1221–1225 (2008).
6. J. Ren, J. Qiu, B. Wu, and D. Chen, "Ultrabroad infrared luminescence from Bi-doped alkaline earth metal germanate glasses," *J. Mater. Res.* **22**(06), 1574–1578 (2007).
7. M. Peng, J. Qiu, D. Chen, X. Meng, I. Yang, X. Jiang, and C. Zhu, "Bismuth- and aluminum-codoped germanium oxide glasses for super-broadband optical amplification," *Opt. Lett.* **29**(17), 1998–2000 (2004).
8. M. Peng, J. Qiu, D. Chen, X. Meng, and C. Zhu, "Superbroadband 1310 nm emission from bismuth and tantalum codoped germanium oxide glasses," *Opt. Lett.* **30**(18), 2433–2435 (2005).
9. X. G. Meng, J. R. Qiu, M. Y. Peng, D. P. Chen, Q. Z. Zhao, X. W. Jiang, and C. S. Zhu, "Near infrared broadband emission of bismuth-doped aluminophosphate glass," *Opt. Express* **13**(5), 1628–1634 (2005).
10. X. G. Meng, J. R. Qiu, M. Y. Peng, D. P. Chen, Q. Z. Zhao, X. W. Jiang, and C. S. Zhu, "Infrared broadband emission of bismuth-doped barium-aluminum-borate glasses," *Opt. Express* **13**(5), 1635–1642 (2005).
11. G. P. Dong, X. D. Xiao, J. J. Ren, J. Ruan, X. F. Liu, J. R. Qiu, C. G. Lin, H. Z. Tao, and X. J. Zhao, "Broadband infrared luminescence from bismuth-doped GeS₂-Ga₂S₃ chalcogenide glasses," *Chin. Phys. Lett.* **25**(5), 1891–1894 (2008).
12. M. A. Hughes, T. Akada, T. Suzuki, Y. Ohishi, and D. W. Hewak, "Ultrabroad emission from a bismuth doped chalcogenide glass," *Opt. Express* **17**(22), 19345–19355 (2009).

13. Y. Fujimoto and M. Nakatsuka, "Infrared Luminescence from Bismuth-Doped Silica Glass," *Jpn. J. Appl. Phys. Part 2 Lett* **40**, L279–L281 (2001).
14. X. Wang and H. Xia, "Infrared superbroadband emission of Bi ion doped germanium-aluminum-sodium glass," *Opt. Commun.* **268**(1), 75–78 (2006).
15. M. Y. Sharonov, A. B. Bykov, V. Petricevic, and R. R. Alfano, "Spectroscopic study of optical centers formed in Bi-, Pb-, Sb-, Sn-, Te-, and In-doped germanate glasses," *Opt. Lett.* **33**(18), 2131–2133 (2008).
16. S. Khonthon, S. Morimoto, Y. Arai, and Y. Ohishi, "Luminescence Characteristics of Te- and Bi-Doped Glasses and Glass-Ceramics," *J. Ceram. Soc. Jpn.* **115**(1340), 259–263 (2007).
17. V. O. Sokolov, V. G. Plotnichenko, and E. M. Dianov, "Origin of broadband near-infrared luminescence in bismuth-doped glasses," *Opt. Lett.* **33**(13), 1488–1490 (2008).
18. I. A. Bufetov and E. M. Dianov, "Bi-doped fiber lasers," *Laser Phys. Lett.* **6**(7), 487–504 (2009).
19. S. V. Firstov, A. V. Shubin, V. F. Khopin, M. A. Mel'kumov, I. A. Bufetov, O. I. Medvedkov, A. N. Guryanov, and E. M. Dianov, "Bismuth-doped germanosilicate fibre laser with 20-W output power at 1460 nm," *Quantum Electron.* **41**(7), 581–583 (2011).
20. V. V. Dvoyrin, V. M. Mashinsky, and E. M. Dianov, "Efficient Bismuth-Doped Fiber Lasers," *IEEE J. Quantum Electron.* **44**(9), 834–840 (2008).
21. S. Kivisto, J. Puustinen, M. Guina, O. G. Okhotnikov, and E. M. Dianov, "Tunable modelocked bismuth-doped soliton fibre laser," *Electron. Lett.* **44**(25), 1456–1458 (2008).
22. A. B. Rulkov, A. A. Ferin, S. V. Popov, J. R. Taylor, I. Razdobreev, L. Bigot, and G. Bouwmans, "Narrow-line, 1178nm CW bismuth-doped fiber laser with 6.4W output for direct frequency doubling," *Opt. Express* **15**(9), 5473–5476 (2007).
23. S. Yoo, M. P. Kalita, J. Sahu, J. Nilsson, and D. Payne, "Bismuth-doped fiber laser at 1.16 μm ," in *Lasers and Electro-Optics, Conference on Quantum Electronics and Laser Science. CLEO/QELS*, 2008), 1–2.
24. J. C. Phillips, "Constraint theory and carrier-type reversal in Bi-Ge chalcogenide alloy glasses," *Phys. Rev. B Condens. Matter* **36**(8), 4265–4270 (1987).
25. K. L. Bhatia, D. P. Gosain, G. Parthasarathy, and E. S. R. Gopal, "On the structural features of doped amorphous chalcogenide semiconductors," *J. Non-Cryst. Solids* **86**(1-2), 65–71 (1986).
26. L. Tichý, H. Tichá, A. Tříska, and P. Nagels, "Is the n-type conductivity in some Bi-doped chalcogenide glasses controlled by percolation?" *Solid State Commun.* **53**(4), 399–402 (1985).
27. V. K. Bhatnagar and K. L. Bhatia, "Frequency dependent electrical transport in bismuth-modified amorphous germanium sulfide semiconductors," *J. Non-Cryst. Solids* **119**(2), 214–231 (1990).
28. S. R. Elliott and A. T. Steel, "Mechanism for Doping in Bi Chalcogenide Glasses," *Phys. Rev. Lett.* **57**(11), 1316–1319 (1986).
29. P. Kounavis, E. Mytilineou, and M. Roilos, "p-n junctions from sputtered $\text{Ge}_{25}\text{Se}_{75-x}\text{Bi}_x$ films," *J. Appl. Phys.* **66**(2), 708–710 (1989).
30. H. Fritzsche and M. Kastner, "The effect of charged additives on the carrier concentrations in lone-pair semiconductors," *Philos. Mag. B* **37**(3), 285–292 (1978).
31. S. Okano, H. Yamakawa, M. Suzuki, and A. Hiraki, "Fabrication of Chalcogenide Amorphous Semiconductor Diodes Using Low Temperature Thermal Diffusion Techniques," *Jpn. J. Appl. Phys.* **26**(Part 1, No. 7), 1102–1106 (1987).
32. S. Okano, M. Suzuki, T. Imura, and A. Hiraki, "Chalcogenide amorphous-semiconductor diodes," *Jpn. J. Appl. Phys. Part 2 Lett* **24**, L445–L448 (1985).
33. S. Okano, M. Suzuki, and M. Suzuki, "Electrical contact properties of metal-chalcogenide amorphous-semiconductor systems," *Jpn. J. Appl. Phys.* **20**(9), 1635–1640 (1981).
34. T. Suzuki and Y. Ohishi, "Ultrabroadband near-infrared emission from Bi-doped $\text{Li}_2\text{O}-\text{Al}_2\text{O}_3-\text{SiO}_2$ glass," *Appl. Phys. Lett.* **88**(19), 191912 (2006).
35. M. Hughes, T. Suzuki, and Y. Ohishi, "Advanced bismuth doped lead-germanate glass for broadband optical gain devices," *J. Opt. Soc. Am. B* **25**(8), 1380–1386 (2008).
36. S. Parke and R. S. Webb, "The optical properties of thallium, lead and bismuth in oxide glasses," *J. Phys. Chem. Solids* **34**(1), 85–95 (1973).
37. B. Denker, B. Galagan, V. Osiko, I. Shulman, S. Sverchkov, and E. Dianov, "The IR emitting centers in Bi-doped Mg-Al-Si oxide glasses," *Laser Phys.* **19**(5), 1105–1111 (2009).
38. M. A. Hughes, T. Suzuki, and Y. Ohishi, "Compositional dependence of the optical properties of bismuth doped lead-aluminum-germanate glass," *Opt. Mater.* **32**(9), 1028–1034 (2010).
39. M. Hughes, T. Suzuki, and Y. Ohishi, "Towards a high-performance optical gain medium based on bismuth and aluminum co-doped germanate glass," *J. Non-Cryst. Solids* **356**(6-8), 407–418 (2010).
40. B. I. Denker, B. I. Galagan, V. V. Osiko, I. L. Shulman, S. E. Sverchkov, and E. M. Dianov, "Factors affecting the formation of near infrared-emitting optical centers in Bi-doped glasses," *Appl. Phys. B.* **98**(2-3), 455–458 (2010).
41. X. Jiang and A. Jha, "An investigation on the dependence of photoluminescence in Bi_2O_3 -doped GeO_2 glasses on controlled atmospheres during melting," *Opt. Mater.* **33**(1), 14–18 (2010).
42. Y. Zhou, N. Gai, and J. Wang, "Comparative investigation on spectroscopic properties of Er^{3+} between Ce^{3+} -doped and B_2O_3 -added bismuth glasses," *J. Phys. Chem. Solids* **70**(2), 261–265 (2009).
43. H. Masai, Y. Takahashi, and T. Fujiwara, "Addition effect of SnO in optical property of Bi_2O_3 -containing aluminoborate glass," *J. Appl. Phys.* **105**(8), 4 (2009).

44. A. Winterstein, S. Manning, H. Ebendorff-Heidepriem, and L. Wondraczek, "Luminescence from bismuth-germanate glasses and its manipulation through oxidants," *Opt. Mater. Express* **2**(10), 1320–1328 (2012).
45. A. Leboutellier and P. Courtine, "Improvement of a bulk optical basicity table for oxidic systems," *J. Solid State Chem.* **137**(1), 94–103 (1998).
46. V. Dimitrov and S. Sakka, "Electronic oxide polarizability and optical basicity of simple oxides. I," *J. Appl. Phys.* **79**(3), 1736–1740 (1996).
47. M. A. Hughes, T. Suzuki, and Y. Ohishi, "Spectroscopy of bismuth doped lead-aluminum-germanate glass and yttrium-aluminum-silicate glass," *J. Non-Cryst. Solids* **356**(44-49), 2302–2309 (2010).
48. J. Ren, J. Qiu, D. Chen, C. Wang, X. Jiang, and C. Zhu, "Infrared luminescence properties of bismuth-doped barium silicate glasses," *J. Mater. Res.* **22**(07), 1954–1958 (2007).
49. W. Xu, M. Peng, Z. Ma, G. Dong, and J. Qiu, "A new study on bismuth doped oxide glasses," *Opt. Express* **20**(14), 15692–15702 (2012).
50. H. Bach, F. K. G. Baucke, and D. Krause, *Electrochemistry of Glasses and Glass Melts, Including Glass Electrodes* (Springer, 2000).
51. M. A. Hamstra, H. F. Folkerts, and G. Blasse, "Materials chemistry communications. Red bismuth emission in alkaline-earth-metal sulfates," *J. Mater. Chem.* **4**(8), 1349 (1994).
52. M. Peng, C. Wang, D. Chen, J. Qiu, X. Jiang, and C. Zhu, "Investigations on bismuth and aluminum co-doped germanium oxide glasses for ultra-broadband optical amplification," *J. Non-Cryst. Solids* **351**(30-32), 2388–2393 (2005).
53. Y. Ohishi, "Novel photonics materials for broadband lightwave processing," in *Optical Components and Materials IV*, Proceedings of the Society of Photo-Optical Instrumentation Engineers (SPIE) 2007, 646908.
54. S. Sumimiya, T. Nanba, Y. Miura, and S. Sakida, "Optical Properties of Bi₂O₃-La₂O₃-Al₂O₃-B₂O₃ Glasses," in *Advances in Glass and Optical Materials II* (John Wiley & Sons, Inc., 2006), pp. 127–133.
55. B. Denker, B. Galagan, V. Osiko, I. Shulman, S. Sverchkov, and E. Dianov, "Absorption and emission properties of Bi-doped Mg-Al-Si oxide glass system," *Appl. Phys. B* **95**(4), 801–805 (2009).
56. M. A. Hughes, T. Suzuki, and Y. Ohishi, "Compositional optimization of bismuth-doped yttria-alumina-silica glass," *Opt. Mater.* **32**(2), 368–373 (2009).
57. J. Ren, Y. Qiao, C. Zhu, X. Jiang, and J. Qiu, "Optical amplification near 1300 nm in bismuth-doped strontium germanate glass," *J. Opt. Soc. Am. B* **24**(10), 2597–2600 (2007).
58. M. Qian, C. Yu, J. Cheng, K. Li, and L. Hu, "The broadband NIR emission properties of Bi doped La₂O₃-Al₂O₃-SiO₂ glass," *J. Lumin.* **132**(10), 2634–2638 (2012).
59. Y. Kim, J. H. Baeck, M.-H. Cho, E. J. Jeong, and D.-H. Ko, "Effects of N²⁺ ion implantation on phase transition in Ge₂Sb₂Te₅ films," *J. Appl. Phys.* **100**(8), 083502 (2006).
60. N. Tohge, T. Minami, Y. Yamamoto, and M. Tanaka, "Electrical and optical properties of n-type semiconducting chalcogenide glasses in the system Ge-Bi-Se," *J. Appl. Phys.* **51**(2), 1048–1053 (1980).
61. J. Málek, J. Klikorka, L. Beneš, L. Tichý, and A. Trřiska, "Electrical and optical properties of Ge₂₀Sb_{15-x}Bi_xBi₆₅ glasses," *J. Mater. Sci.* **21**(2), 488–492 (1986).

1. Introduction

Bismuth-doped glasses can give rise to photoluminescence (PL) at wavelengths ranging from 400 nm [1] to 2500 nm [2], under variation of the pump wavelength and composition of the host glass. A wide variety of traditional glass hosts containing Bi have been investigated to date, mainly silicates [3–5] and germanates [6–8], but also phosphates [9], borates [10], chalcogenides [11, 12] and chlorides [2]. The origin of the infrared emission from Bi-doped glasses remains controversial, with convincing arguments being made for a variety of different emission centers, including Bi⁺ [10], Bi⁵⁺ [13, 14], Bi metal clusters [8], point defects [15] and negatively charged Bi₂ dimers [16, 17]. However, there is a general consensus developing that more than one Bi center is responsible for the observed optical activity of the Bi dopant in glass. Pb doping has also been shown to have very similar absorption and photoluminescence behavior to that of Bi in glasses [15]. Broadband Bi-doped fiber lasers operating at wavelengths between 1150 and 1550 nm [18], with powers up to 20 W [19] and slope efficiencies of up to 30% [20], have been reported. A mode-locked Bi-doped fiber laser with 900 fs pulses has also been demonstrated [21]. Bismuth-doped glasses are therefore, potentially, an extremely important class of material for use in broadband lasers and optical amplifiers. One of the main limitations of Bi-doped fiber lasers fabricated so far is the inability to obtain lasing with doping concentrations more than around 0.005 wt% [22]. This means that the fibers need to be on the order of 100 m in length, which causes problems of background loss and nonlinearities. Absorption tails located close to lasing wavelengths cause additional losses [23]. The presence of Bi centers not involved in the lasing process

could cause concentration quenching and absorption losses. Therefore, an understanding of the nature of the Bi centers, and the ability to control which Bi centers are present, is critical for the ability to increase doping concentration, reduce losses and bring the performance of Bi-doped fiber lasers in line with that of rare-earth-doped fiber lasers.

Chalcogenide glasses are a broad class of increasingly important technological materials used in phase-change memories, solar cells, sensors and non-linear optical devices. They almost invariably display p-type electronic conductivity, and are known to remain p-type when melted with common donor atoms. The ability to reverse the carrier type in these glasses would enable electronic devices to be integrated with other chalcogenide-glass-based devices and may enable the fabrication of LEDs and laser diodes that emit at novel wavelengths.

Bi and Pb are the only known dopants to cause carrier-type reversal (CTR) in chalcogenide glasses by melt doping, mainly in germanium chalcogenides. The origin of this carrier-type reversal is also disputed. Phillips proposed a model for the microscopic structure of Bi-modified $\text{Ge}_x\text{B}_{1-x}$ (B = S, Se or Te) glass as Bi_2B_3 clusters with a tetradymite-like structure embedded in a $\text{Ge}_x\text{B}_{1-x}$ matrix [24]. This was based on differential thermal analysis (DTA) [25] and penetration probe [26] measurements which indicated a phase separation in the Bi-modified glasses. A.C. measurements indicate that these clusters may have n-type defects situated at excess S^- atoms on cluster surfaces; these defects may be taking part in a single-polaron hopping process [27]. However, on the basis of EXAFS measurements, Elliott *et al* argued that Bi is only 3-fold coordinated, and that the glasses were homogeneous without Bi_2S_3 clusters [28], and that the mechanism of CTR is due to the presence of charged Bi atoms which suppress the concentration of positively charged chalcogen defects at the expense of negatively charged defects. In 1989, a p-n junction based on the Ge-Se-Bi glass system was fabricated [29]. However, since this time there have not been significant strides in increasing the performance of these p-n junctions, which may be related to the lack of understanding of the physical process that underlies carrier-type reversal in these glasses.

Conventionally, Bi and Pb dopants are introduced into the glass melts ('melt-doping'). We define melt-doping as an equilibrium doping method because the dopants are able to react with the glass material, above the glass-transition temperature, T_g , for sufficient time for the dopants to achieve their lowest energy bonding configuration. We define non-equilibrium doping as the inclusion of a dopant into the glass matrix below T_g . Ion implantation is a precise, non-equilibrium doping technique which is essential to the fabrication of most modern integrated circuits (ICs). It is relevant to Bi-doped glasses because it may allow control over which Bi centers are present in the glass. It is also relevant for the development of high-performance electronic devices based on Bi-doped glasses because it is the most precise doping technique in use today, and it may be possible to reverse the carrier type of chalcogenide glasses by impurity doping under non-equilibrium conditions [30], as has been shown for Cd, Al, Zn and Mg (non-equilibrium) diffusion-doped $\text{As}_2\text{Se}_2\text{Te}_1$ glass [31–33]. In this work, we report, for the first time, that the order of the reaction which generates optically active Bi centers varies significantly between different glass hosts. We also report, for the first time, PL from Bi- and Pb-implanted glasses, some of which have compositions very close to those in which carrier-type reversal has been reported, and suggest that these phenomena are produced by the same, or a similar, active center. If our hypothesis is correct, it may assist in hastening the elucidation of the origin of these phenomena.

2. Experimental

2.1 Sample preparation

A gallium lanthanum sulphur oxide (GLSO) sputtering target was prepared by mixing 70% gallium sulphide, 24% lanthanum sulphide and 6% lanthanum oxide in a dry-nitrogen purged glove box. The raw materials were melted for 24 hours in dry argon, in 2 inch diameter

vitreous carbon crucibles, annealed at the glass-transition temperature and then sliced to form a 3mm thick sputter target. We sputtered 100 nm thick films of GLS onto 1 μ m thick thermally oxidized SiO₂ on Si substrates. The RF sputtering power was 60W, with an Ar flow of 15 SCCM. Details of the fabrication of bulk Bi-doped GLSO [12], SiAlLiO [34] and GeAlPbO [35] can be found elsewhere. The Ge₃₃S₆₇ and Ga₅Ge₂₅S₇₀ bulk samples were synthesized from high-purity elemental Ge (5N purity), Ga (7N purity) and S (5N purity) in evacuated (10⁻³ Pa) and sealed fused silica ampoules placed in a rocking furnace and heated to 975 °C for 24 hours. The melt was then air-quenched to room temperature. The obtained glass samples were annealed at T_g-10 °C for 2 hours, and then cut and polished into samples around 10x10x1mm in size.

Bismuth and lead ions were implanted using a Danfysik ion implanter. The ion energy (keV) and dose (ions/cm²) for the Bi implants were: 190, 1x10¹⁴; 190, 1x10¹⁵ and 350, 1x10¹⁶. For Pb, they were 350, 3x10¹⁵. During implantation, the samples were mounted on a carousel holder held at ambient temperature, and the beam current was kept below 1 μ A/cm² to avoid beam heating of the targets.

2.2 Sample characterization

Photoluminescence (PL) spectra of bulk samples were obtained by exciting with a 808 nm laser diode, or 514 nm Ar- ion laser. The emission was dispersed by a Jasco CT-25C monochromator which used a 600 or 1200 lines/mm grating. The slit width was ~2.5 mm, which corresponded to a resolution of ~10 nm. The stray excitation light was blocked with appropriate long-pass filters. Detection was realized with a Hamamatsu H9170 NIR photomultiplier tube (PMT), Newport Si, or InGaS detectors, coupled with standard phase-sensitive detection. All spectral measurements were corrected for the wavelength-dependent response of the measurement system by calculating a correction spectrum (C(λ)), with C(λ) = I_{cal}(λ)/I_{meas}(λ), where I_{meas}(λ) is the luminescence spectrum of an Ushio calibrated white-light source measured by the detection system and I_{cal}(λ) is the luminescence spectrum of the calibrated white-light source supplied by the manufacturer. Due to their weak emission, PL spectra of implanted samples were taken on a Renishaw 2000 microRaman system incorporating a Si CCD detector array, with a detection range of 400 – 1100 nm, and 514 or 782 nm excitation laser lines. A 50x microscope objective was used to focus the excitation onto the implanted sample surface. Several spectra were taken at different positions on the sample and then averaged. It was found that the variation in PL intensity between different positions on the same sample was less than 5%. This technique can therefore be used to compare the relative PL intensity between different implants. We also measured the PL from unimplanted samples to account for any PL that could be coming from the unimplanted film or substrate. These spectra were then subtracted from the PL spectra of the implanted samples. The PL intensity of unimplanted samples was less than around 5% of that of the implanted samples in the thin-film samples, and less than 25% in the bulk samples. Spectra were corrected by measuring the broadband PL of a Bi-doped glass with a known spectral luminance. Ripples in some of the PL spectra measured on the Raman system are an artifact caused by the various filters. Differential thermal analysis (DTA) measurements were taken using a Rigaku Thermo Plus TG-DTA. Rutherford back-scattering (RBS) measurements were made on a 2MV Tandatron accelerator using 2 MeV He beams.

3. Results and discussion

3.1 Review of bulk oxides and chalcogenides

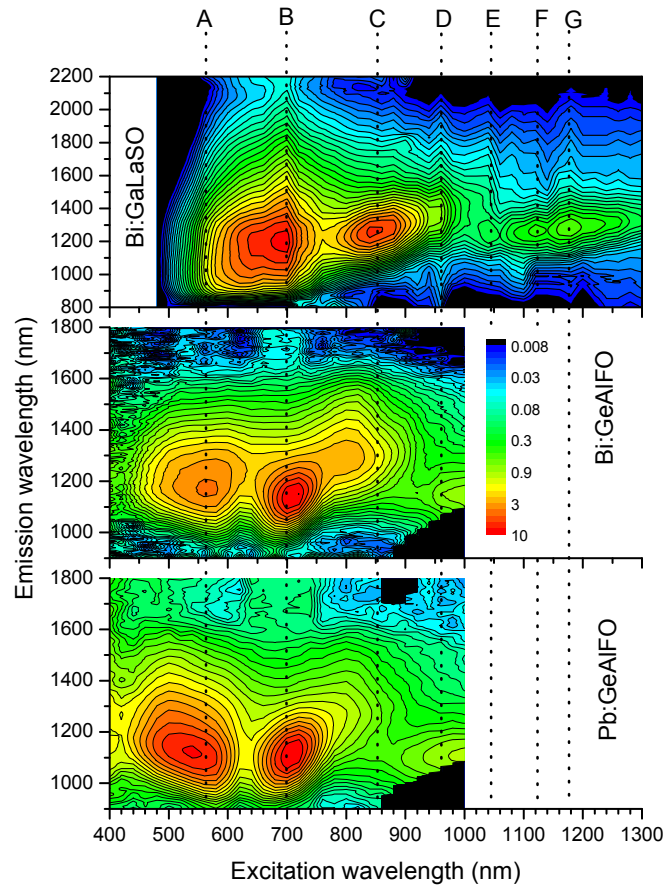


Fig. 1. Contour plots of PL emission from Bi-doped GLSO, after [12], and Bi- and Pb-doped germanate bulk glasses, after [15]. The intensity is plotted on a log scale.

Figure 1 shows contour plots, which are comprised of a series of PL spectra over a range of excitation wavelengths, of $\text{Ga}_{28}\text{La}_{12}\text{S}_{56}\text{O}_4\text{Bi}_{0.4}$ (Bi:GLSO), after [12], $\text{Ge}_{28}\text{O}_{56}\text{F}_{11}\text{Al}_4\text{Bi}_{0.6}$ (Bi:GeAlFO), and $\text{Ge}_{28}\text{O}_{56}\text{F}_{12}\text{Al}_4\text{Pb}_{0.3}$ (Pb:GeAlFO), after [15]. These contour plots can be used to determine the position of absorption and PL bands. Strong absorption/PL bands show up clearly as islands on the contour plot; weaker absorption/PL bands show up as kinks and bends in the contour lines. In Fig. 1, we identified seven absorption/PL bands in Bi:GLSO, marked A-G. The positions of these bands for all three glasses are given in Table 1. Band A is rather indistinct in Bi:GLSO, which may be caused by the strong band-edge absorption of GLSO in this region. However, there is a clear change in direction of the contour lines at 565 nm, indicating the presence of an absorption/PL band, which lines up almost exactly with the strong band in Bi:GeAlFO. Band D is evident only as a kink in contour lines in Bi:GeAlFO at 960 nm, and is not evident in Pb:GeAlFO. Much of band E is missing in the germanate glasses; however, it is not much greater than 1000 nm. We find that the positions of 5 absorption/PL bands are approximately the same in Bi- and Pb-doped germanate glass and

Bi-doped chalcogenide glass, indicating that they are related to essentially the same optical center. Similar absorption and emission properties were also observed in Bi- and Pb-doped calcium phosphate and sodium silicate glasses [36]. The origin of this similarity is intriguing. Similar NIR PL bands have been reported from Bi, Pb, Sb and Sn doped germanate glasses [15], and since spin-orbit constants are so dissimilar for these elements, it has been argued that the NIR PL did not originate from dopant centers. We suggest, however, that there may be similarities in the energy level structure of complex clusters of these elements, which could produce similar NIR PL bands.

Table 1. Positions of absorption/PL bands (nm) for Bi:GLSO, Bi:GeAlFO and Pb:GeAlFO

Glass		Band						
		A	B	C	D	E	F	G
Bi:GLSO	Abs.	565	700	855	960	1045	1125	1180
	PL	1080	1175	1260	1360	1250	1260	1270
Bi:GeAlFO	Abs.	560	710	800	960	>1000	-	-
	PL	1170	1140	1280	1350	1140	-	-
Pb:GeAlFO	Abs.	540	710	820	-	>1000	-	-
	PL	1120	1110	1260	-	1120	-	-

3.2 Reaction mechanism in bulk oxide glasses

Previous work has shown clearly that Bi centers in oxide glasses are generated by a redox reaction during the glass-melting process. This is because the strength of the Bi absorption bands have a dependence on melting temperature [37], melting time [38, 39] and oxygen partial pressure [40, 41]. However, Fourier transform infra-red (FTIR) [42] and x-ray photoelectron spectroscopy (XPS) [43] measurements of Bi₂O₃-doped glasses indicate the presence of Bi₂O₃. The addition of just 0.2% of the oxidizer, CeO₂, to 70.5GeO₂-24.5Bi₂O₃-5WO₃ glass removed the strong 500 nm Bi-related absorption band [44], indicating that only a very small proportion of Bi₂O₃ converts to optically active Bi centers.

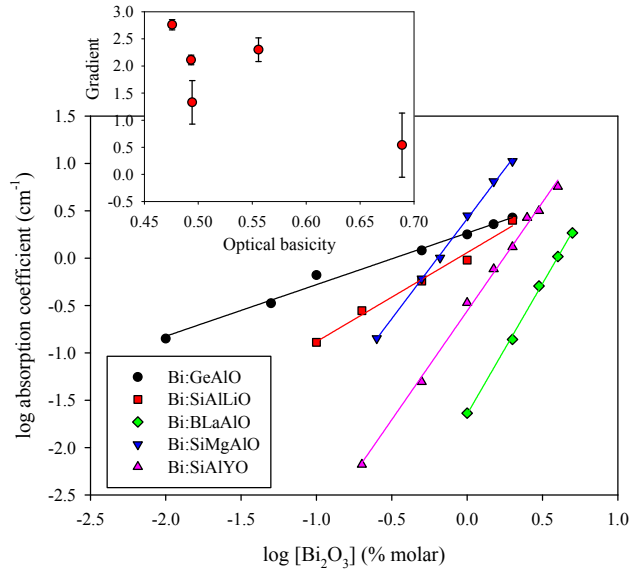


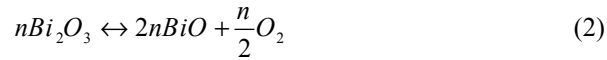
Fig. 2. Log-log plot of the absorption coefficient of the Bi-related 500 nm absorption band as a function of Bi₂O₃ doping concentration for various oxide glasses. Solid lines are linear fits. The inset shows the gradient of the fits as a function of the optical basicity of the glass hosts; errors were estimated from the R² value of the linear fits.

Figure 2 shows the log of the absorption coefficient of various bismuth-doped oxide glasses as a function of the log of the Bi₂O₃ doping concentration. The strength of the Bi absorption band is directly proportional to the concentration of the, as-yet, undetermined optically active Bi centers (Bi_c). The gradient of the straight lines in Fig. 2 gives the power-law factor that relates [Bi_c] to [Bi₂O₃], i.e. the reaction order. The power-law factors are given in Table 2; they indicate that the reaction order varies with the glass host. There does not seem to be a dependence of the reaction order on melting conditions. The Bi absorption strength of germanate glasses increases with melting duration [38, 39]; we can suppose, therefore, that reactions generating Bi_c have not reached equilibrium. Optical basicity (Λ) is a term used to define the electron-donating power of the oxygen in an oxide glass [45]. We calculated the optical basicity of all the glass hosts in Fig. 2 using Eq. (1):

$$\Lambda = X_A \Lambda(A) + X_B \Lambda(B) + \dots \quad (1)$$

where X_A, X_B... are the molar proportions contributed by the constituent oxides, A, B, ... to the total oxide content. Λ(A), Λ(B),... are the optical-basicity values of the individual oxides published by Dimitrov et al [46]. The optical basicity is plotted against the gradients of the linear fits, i.e. the reaction order, in the inset of Fig. 2. This plot indicates that increasing optical basicity reduces the order of the reaction that generates Bi_c. It has been shown that increasing the optical basicity of the glass host reduces the strength of Bi absorption [47, 48]. Increases in Λ should increase the proportion of the upper oxidation state of dopant metal ions, since they require more negative charge to balance their positive charge than do lower oxidation-state ions.

Reaction orders with values <1 indicate the presence of intermediate reaction steps. The observation that Bi absorption decreases by a power law with increasing oxygen partial pressure [40], indicates that oxygen must be liberated in the reaction to generate Bi_c, which indicates that the intermediate reaction step is the decomposition of Bi₂O₃ into its sub-oxide, BiO. The fact that reaction orders with values > 1 are observed indicates that Bi must be clustering. There is also a general consensus that at least two different types of Bi centers are present in Bi-doped glasses [44, 49]. We therefore propose the following redox reactions, Eqs. (2-4), to generate the optically active Bi centers (Bi²⁺ and Bi_n clusters):



The equilibrium constant (K_c) of a redox pair in glass melts has been shown to be a function of the glasses' optical basicity, of the form: logK_c = a-bΛ [50], where a and b are constants. The reactions in Eqs. (2-4) are assigned the equilibrium constants K_{c1}, K_{c2} and K_{c3}, respectively, which are related to Λ by the constants a₁ and b₁, a₂ and b₂, and a₃ and b₃, respectively. In sequential reactions like those in Eqs. (2-4), the overall reaction order is determined by which reaction has the slowest, rate-determining step. The equilibrium positions, and therefore reaction rates, depend as a power law on Λ. If, for example, a₁<a₂ and b₁<b₂, then as Λ is increased, the rate-determining step for Bi²⁺ could change from Eq. (3) to Eq. (2), and the reaction order would change from 0.5 to 1. If we assume that Bi₂ clusters are generated as in Eq. (4), and b₁, b₂<0, b₃>0, then the reaction order will be ~2 at lower Λ. So, as long as we assume that Bi²⁺ and Bi_n clusters both generate 500 nm absorption bands, then this model can explain reaction orders in the range of 0.5 to >1, and their dependence on Λ. Two absorption bands at ~500 nm can occasionally be resolved in Bi-doped glasses [41];

however, usually only one can be resolved. It may be the case that two absorption bands at ~500 nm exist in all Bi-doped glasses, but their proximity and differences in strength mean only one band can be resolved. These two bands could therefore be the two Bi centers, Bi^{2+} and Bi_n clusters, that we suggest in our model. As shown in Fig. 7, green excitation of Bi-doped oxide glasses often results in characteristic red and NIR PL bands; these PL bands may originate from different Bi centers [49]. Red emission with a decay time of 4 μs has been reported in $\text{MSO}_4\text{:Bi}$ ($M = \text{Ca}, \text{Sr}, \text{Ba}$) crystals and attributed to Bi^{2+} [51]. We therefore assign the red and NIR PL bands to Bi^{2+} and Bi_n clusters, respectively. In Bi:SiMgAlO glass under green excitation, red PL intensity did not increase with Bi_2O_3 content, whereas NIR PL intensity was proportional to the Bi absorption strength; this suggests that there are limited vacancies for Bi^{2+} which become filled at low doping concentrations. Our model seems to predict that, in glasses with high Λ and with low reaction order, the red/NIR PL intensity ratio should be higher than in glasses with low Λ and high reaction order, although we do not yet have any data to test this.

Table 2. Power-law factor relating absorption to Bi_2O_3 doping concentration in oxide glasses

Glass	Composition (% molar)	Melt temperature (°C), time (min)	Power-law factor	Ref
Bi:GeAlO	97-xGeO ₂ :3Al ₂ O ₃ :xBi ₂ O ₃	1540, 20	0.54	[52]
Bi:SiAlLiO	64-xSiO ₂ :23Al ₂ O ₃ :13Li ₂ O:xBi ₂ O ₃	1600, 120	1.33	[53]
Bi:BLaAlO	78B ₂ O ₃ :22La ₂ O ₃ :6Al ₂ O ₃ :xBi ₂ O ₃	1250, 40	2.76	[54]
Bi:SiMgAlO	55.6SiO ₂ :22.2Al ₂ O ₃ :22.2MgO:xBi ₂ O ₃	1550, 240	2.11	[55]
Bi:SiAlYO	64.5-xSiO ₂ :22.5Al ₂ O ₃ :13Y ₂ O ₃	1550, 60	2.30	[56]

Figure 3 shows the DTA scans of Bi-doped germanate glasses containing 4 and 10 mol % PbO. The Bi content is low enough not to affect the measurement. The scans show that there is only one phase present in the glass containing 4% PbO; however, in the 10% PbO glass, there are clearly two crystallization temperatures (T_c) and two melting temperatures (T_m), and possibly two glass-transition temperatures (T_g), indicating a phase separation. This could be seen as being analogous to the phase separation observed in Bi-doped GeS glasses displaying carrier-type reversal when the Bi content is increased past 11 mol% [25, 26]. The addition of other modifiers to germanate glasses usually does not cause phase separation; for example, only one T_g and T_c were observed in $1\text{Bi}_2\text{O}_3\text{:}5\text{Al}_2\text{O}_3\text{:}20\text{SrO:}75\text{GeO}_2$ glass [57]. Thermal analysis of high Bi-content oxide and chalcogenide glasses is a priority for making comparisons to the phase separation observed in Bi:GeS.

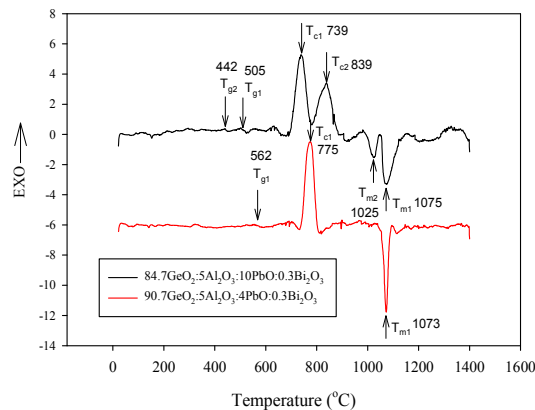


Fig. 3. DTA scan of Bi-doped lead germanate glasses.

3.3 Ion-implanted chalcogenides

Figure 4 shows ‘transport of ions in matter’ (TRIM) computer simulations of the implanted-ion depth distribution of the various implants and target samples used in this study, along with an RBS measurement of the depth distribution of Pb in a GLSO thin film, implanted with a 3×10^{15} ions/cm² dose and an energy of 350 keV. TRIM simulations give distributions in ion/cm³, which we converted to at.% using the measured density of the bulk glasses. The simulations show that the peak doping concentrations for a 1×10^{16} ions/cm² dose is around 3-4 at.%, reducing approximately linearly with dose, even though the energy was varied. Comparing the RBS measurement to the appropriate simulation indicates that the area under the distributions (equivalent to dose) is larger in the simulation; this indicates that the density of the film is higher than the bulk density we used to convert to at.%. RBS analysis also indicated that the composition of the film was Ga₂₆La₁₂S₄₅O₁₇, whereas the sputtering target had a composition of Ga₂₆La₁₄S₅₇O₃, indicating preferential sputtering of O, and/or post-deposition atmospheric oxidation of the film. The measured depth profile has a significantly shorter range (40 nm) than the simulated profile (80 nm), indicating that the TRIM software overestimates the penetration of the ions due to higher densities or other unknown material effects, or significant sputtering of the film is occurring during implantation. However, sputter markers indicated no decrease in depth, greater than the measurement resolution of 5 nm, between implanted and unimplanted regions. This may be due to implantation-induced expansion of the film, since we would expect measurable sputtering at this dose. In summary, peak concentrations may be slightly lower, and ion ranges significantly lower, than found in the simulations.

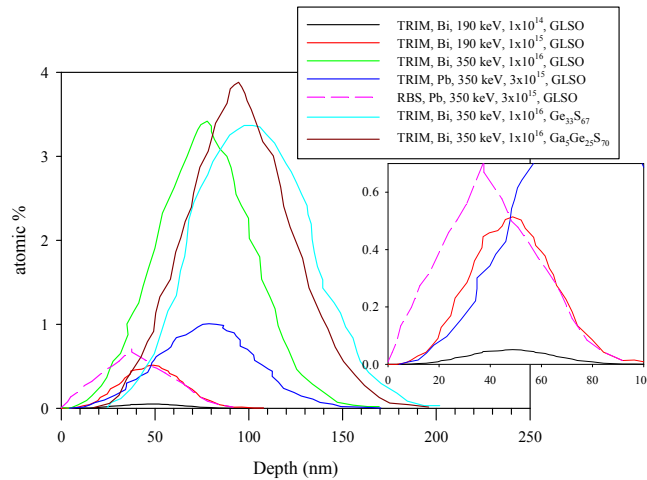


Fig. 4. TRIM simulation of Bi- and Pb-implanted GLSO, GeS and GaGeS glass at various doses and energies, and RBS profile of Pb implanted in GLSO thin film. Inset shows a close-up of the lower dose samples.

Figure 5(a) shows the PL spectra of Bi- and Pb-implanted GLSO films at various doses, excited at 782 nm. The Bi implants all display a PL peak at 820 nm, with a shoulder at 920 nm at low doses. The Pb implant has a similar peak at 860 nm; this is analogous to the similarity between Bi- and Pb-doped germanates. The PL intensity dependence on dose is super-linear, so we plotted the log of the integrated PL intensity (I) against the log of the Bi implant dose in Fig. 5(b) and found that it has a power-law dependence on dose (d): $I \propto d^{1.4}$. If we assume that the PL efficiency does not decrease with dose (which it should not, because this would lead to a non-power-law dependence), then this power-law dependence can be seen as being analogous to the power-law dependence of Bi absorption on Bi content in oxide glasses, shown in Fig. 2, and hence provides evidence for the existence of Bi clusters in the

implanted films. We also extracted the dependence of PL intensity on Bi_2O_3 content in $\text{La}_2\text{O}_3\text{-Al}_2\text{O}_3\text{-SiO}_2$ glass, from Fig. 2 in ref [58], plotted this on Fig. 5(b) also, and found a similar power-law dependence, again linking Bi-doped chalcogenides and oxides.

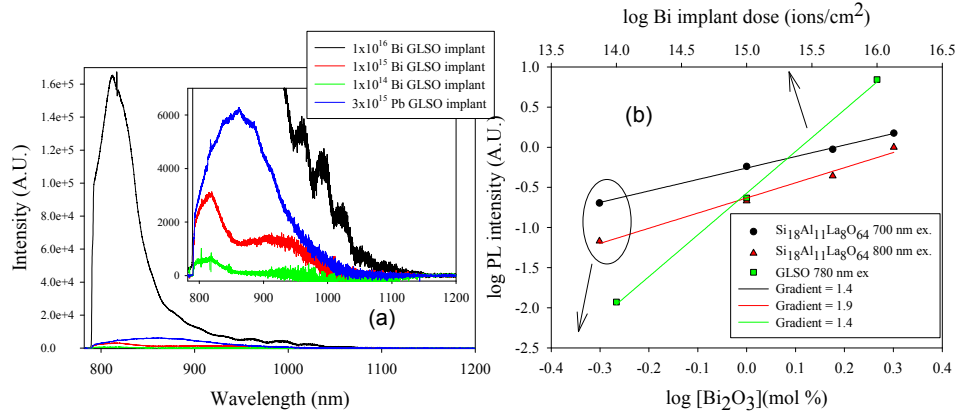


Fig. 5. (a) PL spectra of Bi- and Pb-implanted GLSO thin films at various doses. Excitation was at 782 nm. The inset shows a close-up of low PL intensities. (b) log-log plot showing the integrated PL intensity against Bi_2O_3 content in $\text{La}_2\text{O}_3\text{-Al}_2\text{O}_3\text{-SiO}_2$ glass, after [58], and dose in Bi-implanted GLSO thin films.

Figure 6 shows the PL spectra of 3×10^{15} ions/cm² Pb-implanted GLSO thin film (0.7 at.% peak Pb concentration), compared to bulk Bi- and Pb-doped germanates and GLSO, excited at 782 or 808 nm. The Pb-implanted GLSO has a very similar PL spectrum to Pb-doped germanate glass ($\text{Ge}_{29}\text{O}_{66}\text{Al}_3\text{Pb}_2$), which again indicates the existence of similar Pb centers in Pb-doped chalcogenide and oxide glasses. The narrow PL peak at 860 nm is rather uncharacteristic of Bi- and Pb-doped glasses excited at around 800 nm; indeed, when the $\text{Ge}_{29}\text{O}_{66}\text{Al}_3\text{Pb}_2$ glass is doped with 0.3 at% Bi, the PL intensity increases by around 100 fold and switches to the characteristic broad PL at ~1200 nm. A different Pb-doped germanate glass ($\text{Ge}_{28}\text{O}_{56}\text{F}_{12}\text{Al}_4\text{Pb}_{0.3}$) displays the characteristic broad PL at ~1200 nm, rather than the narrow 860 nm PL; this could be due to the addition of F, or the lower doping concentration. The composition of the bulk Bi-doped GLSO ($\text{Ga}_{28}\text{La}_{12}\text{S}_{42}\text{O}_{18}\text{Bi}_{0.4}$), is very similar to the composition of the 1×10^{15} ions/cm² Bi-implanted GLSO film ($\text{Ga}_{26}\text{La}_{12}\text{S}_{45}\text{O}_{17}\text{Bi}_{0.5}$). However, the PL spectra are rather different: bulk Bi:GLSO also has broad PL at ~1200 nm, whereas the 1×10^{15} ions/cm² Bi-implanted GLSO film exhibits a narrow PL peak at 820 nm, which is associated with $\text{Ge}_{29}\text{O}_{66}\text{Al}_3\text{Pb}_2$ bulk glass. This result is significant because it indicates that ion implantation is able to generate new and different Bi centers, which are not present in a sample whose dopants are introduced during melting.

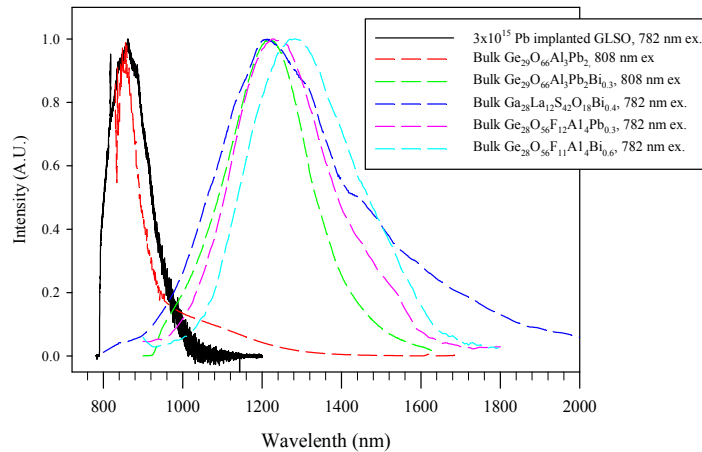


Fig. 6. PL spectra of Pb-implanted GLSO thin film, compared to various Pb- and Bi-doped germanate and GLSO bulk glasses, excited at around 800 nm. Spectra for $\text{Ge}_{28}\text{O}_{56}\text{F}_{12}\text{A}_{14}\text{Pb}_{0.3}$ and $\text{Ge}_{28}\text{O}_{56}\text{F}_{11}\text{A}_{14}\text{Bi}_{0.6}$ are after [15]

Figure 7 shows the PL spectra of Bi- and Pb-implanted GLSO thin films at various doses, along with bulk Bi-doped GLSO and $\text{Li}_2\text{O}-\text{Al}_2\text{O}_3-\text{SiO}_2$ (LAS) glass, excited at 514 nm. Bulk Bi:GLSO exhibits a PL peak at 950 nm. However, the 1×10^{14} ions/cm² Bi-implanted GLSO has a characteristic red PL band, peaking at 700 nm, which is commonly observed in Bi-doped oxide glasses under green excitation [40]. The spectrum of the Bi:LAS glass in Fig. 7 also has a 700 nm PL band, which is very similar to that of the 1×10^{14} ions/cm² Bi-implanted GLSO. Comparing the 1×10^{15} ions/cm² Bi implant to bulk Bi:GLSO (which have very similar compositions) indicates that the 1×10^{15} ions/cm² Bi implant has the 700 nm PL band associated with oxide glasses, and the 950 nm PL band observed in bulk Bi:GLSO, in equal intensities. If we extend our model of oxide glasses, in which red and NIR PL result from Bi^{2+} and Bi_n clusters, respectively, to Bi:GLSO, then implanted Bi is more likely to be incorporated as Bi^{2+} than melt-doped Bi. The 700 nm PL band remains approximately constant for 1×10^{14} and 1×10^{15} ions/cm² Bi implants, which is similar to the effect discussed earlier for Bi:SiMgAlO [40]. For the 1×10^{16} ions/cm² Bi implant, the 700 nm PL band becomes much stronger and broader. We were unable to detect any NIR PL from the implanted samples using the standard measurement system that we used for our bulk samples.

During ion implantation, accelerated ions are decelerated by collisions with the nuclei, and electronic clouds, of atoms in the target. After a series of collisions, the implanted ion comes to rest. These collisions result in the displacement of individual atoms, which causes damage to the atomic structure of the target. In silicon IC manufacture, this damage is usually relieved by subsequent annealing above the crystallization temperature. This annealing activates the dopant by allowing them to move from an interstitial site to a lattice site. Similarly to ion-implanted Si, we expect that ions implanted into chalcogenide glasses will initially enter interstitial sites. XPS and NEXAFS measurements of N_2 -implanted and nitrogen-codeposited $\text{Ge}_2\text{Sb}_2\text{Te}_5$ amorphous chalcogenide films indicated that implanted N tended to accumulate in interstitial sites compared to codeposited N_2 [59]. This indicates that Bi^{2+} associated with Bi-implanted GLSO may be interstitial. 3×10^{15} ions/cm² Pb-implanted GLSO has a single 700 nm PL band; however, since we do not have an equivalent bulk Pb:GLSO glass with which to compare, it is difficult to say if this PL band is caused by implantation or not. However, we would expect bulk Pb:GLSO to have a similar PL spectrum to Bi:GLSO, based on the similarities between the two dopants that we have reported so far. We assign this band to Pb^+ , which is isoelectronic with Bi^{2+} .

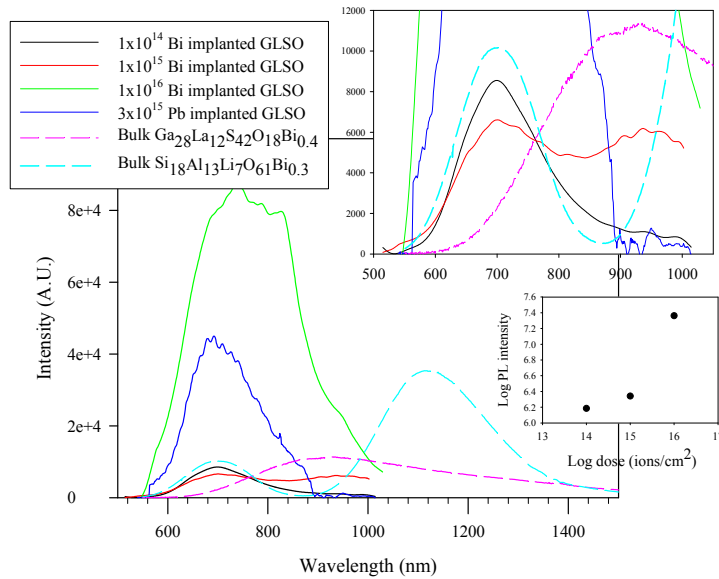


Fig. 7. PL spectra of Bi- and Pb-implanted GLSO films at various doses, and bulk Bi-doped GLSO and LAS glass, excited at 514 nm. The PL intensities of the implanted films are plotted relative to each other, the bulk samples are not. The upper inset shows a close-up of the lower intensity spectra. The lower inset shows a log-log plot showing the integrated PL intensity against Bi dose.

Bi- and Pb-doped chalcogenides are the only melt-doped chalcogenide glasses in which carrier-type reversal has been observed. Investigators of this phenomenon have usually fabricated a series of Bi- or Pb-doped chalcogenide glasses in which the doping content is increased, and measured the thermopower as a function of dopant content. In Bi-doped GeGaS glass, the addition of Bi caused a red-shift in the absorption edge, rather than the appearance of characteristic Bi absorption bands observed in oxide glasses [11]. In fact, the addition of just 0.15 at.% Bi caused a red-shift in the band edge of around 100 nm. A similar red-shift is observed when Bi is added to GeB (B = S, Se, Te) glasses in which CTR is observed [60], and this red-shift is associated with the CTR. Figure 8(a) shows characteristic Bi-related PL from a Bi-doped GeGaS glass ($\text{Ge}_{23}\text{Ga}_{12}\text{S}_{64}\text{Bi}_1$) [11]; at lower Bi concentrations, the PL peak is very similar to a Bi-doped germanate glass. With increasing Bi concentration, the PL becomes significantly weaker and shifts to longer wavelengths. This is probably related to the large red-shift in band edge caused by the addition of Bi. The composition of this glass is very similar to those of glasses in which CTR has been observed ($\text{Ge}_{20}\text{Sb}_{11}\text{S}_{65}\text{Bi}_4$ and $\text{Ge}_{20}\text{S}_{73}\text{Bi}_7$), as shown in Fig. 8(b). It is therefore reasonable to assume that similar Bi centers are generated in glasses displaying CTR and PL. Since PL in Bi-doped glasses is widely thought to originate from multiple Bi centers, it is likely that one or more of these centers causes the CTR. The observation of NIR PL would suggest this center is Bi clusters.

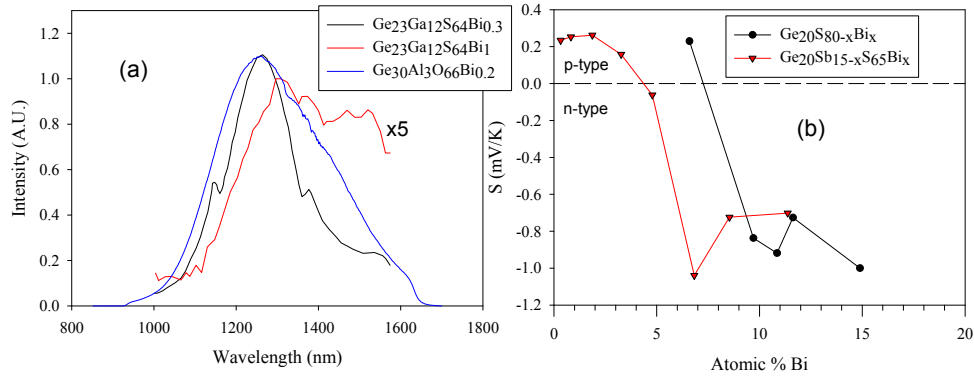


Fig. 8. (a) PL spectra of Bi-doped GeGaS, after [11], and Bi-doped germanate glass, with 808 nm excitation. (b) Thermopower as a function of Bi content in GeS glass, after [26], and in GeSbS glass, after [61].

Figure 9 shows the PL spectra, excited at 514 nm, of 1×10^{16} ions/cm² Bi-implanted bulk Ge₃₃S₆₇ and Ga₅Ge₂₅S₇₀ glass. The Bi-implanted regions should have compositions of Ge₃₃S₆₇Bi_{3.4} and Ga₅Ge₂₅S₇₀Bi_{3.8}. These compositions are even closer to those in which CTR has been observed - see Fig. 8(b). Both glasses display characteristic red Bi PL, indicating the presence of interstitial Bi²⁺, peaking at 670 nm in Ge₃₃S₆₇ and at 700 nm in Ga₅Ge₂₅S₇₀, along with an unknown peak at 885 nm. The observation of both red and NIR PL bands in glasses with compositions close to those in which CTR has been reported indicated that both interstitial Bi²⁺ and Bi clusters are involved in CTR.

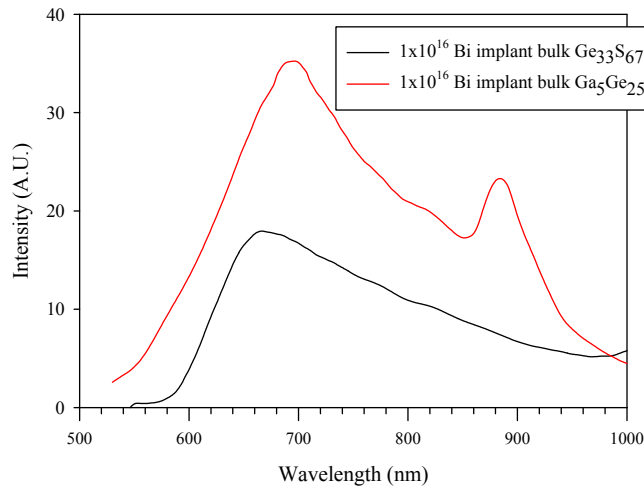


Fig. 9. PL from Bi-implanted bulk GeS and GaGeS glass, excited at 514 nm

4. Conclusions

We determined the reaction order for the generation of Bi centers in various oxide glass hosts by extracting absorption data from previously published work, and measuring the gradient (equivalent to the power-law factor) of a double-logarithmic plot of Bi-related absorption coefficient against Bi₂O₃ doping concentration. The reaction order in Bi-doped oxide glasses decreased with increasing optical basicity of the glass host. A sequential redox reaction involving the decomposition of Bi₂O₃ into BiO, then Bi_n clusters, can explain a reaction order

dependence on optical basicity. We suggest that red and NIR PL bands result from Bi^{2+} and Bi_n clusters, respectively. Comparing contour plots of PL spectra at various excitation wavelengths of Bi-doped chalcogenide, Bi-doped germanate and Pb-doped germanate glasses, indicates that five absorption/PL bands are in approximately the same position. This suggests that very similar active centers are present in Bi- and Pb-doped oxide and chalcogenide glasses.

When excited at 782 nm, Bi- and Pb- implanted GaLaSO thin films display PL bands centered at 820 and 860 nm, respectively. The intensity (I) of the 820 nm PL band has a power law dependence on Bi dose (d) of $I \propto d^{1.4}$; a similar power-law dependence was presented for a Bi melt-doped oxide glass. When excited at 514 nm, Bi-implanted GaLaSO thin films display a PL band at 700 nm, which is not present in a Bi melt-doped chalcogenide glass having a similar composition to the implanted glass. This indicates that new Bi centers are formed through implantation, which are absent in the melt-doped glasses. This has important implications for Bi-doped glass lasers, in which the control of Bi centers is critical for improving performance. We report Bi-related red PL bands in Bi-implanted bulk $\text{Ge}_{33}\text{S}_{67}$ and $\text{Ga}_5\text{Ge}_{25}\text{S}_{70}$ glasses, and highlight NIR PL bands in $\text{Ge}_{23}\text{Ga}_{12}\text{S}_{64}\text{Bi}_1$ glass; all of which have very similar compositions to those in which carrier-type reversal has been observed. This indicates that Bi-related PL and carrier-type reversal may be caused by the same Bi centers, which we suggest are interstitial Bi^{2+} and Bi clusters.

Acknowledgments

We would like to thank Prof. Guoping Dong and Dr. Mikhail Sharonov for supplying data from their publications. This work was supported by the UK EPSRC grants EP/I018414/1, EP/I019065/1 and EP/I018050/1.